Varactor-Tuned Active Notch Filter With Low Passband Noise and Signal Distortion

Christen Rauscher, *Fellow, IEEE*

***Abstract*—The frequency-tunable band-reject filter described in this paper is designed to suppress signal interference in receivers of frequency-agile systems, while offering maximum transparency at passband frequencies. The presented solution is based on a new channelized-active-filter architecture in which the portion of the circuit that determines passband behavior is free of semiconductor devices. This permits passband residual noise and intermodulation distortion to be reduced to that of a simple nonresonant passive network. The concept is demonstrated with a varactor-tuned hybrid-integrated filter whose 40-dB-deep rejection notch of constant 70-MHz width can be tuned over a 9.5–10.5-GHz frequency span. Included are measurements of pertinent small-signal transfer characteristics and noise properties, as well as detailed assessments of nonlinear effects, such as third-order intermodulation distortion and compression of notch depth as a function of drive level.**

***Index Terms*—Band reject, channelized, microwave active filter, miniature, notch, tunable.**

I. Introduction

THE competition among commercial and military high-frequency systems for portions of the available spectrum is placing evermore stringent demands on filters, tasked with separating desired signal information from increasingly dense electronic clutter. Filters must provide not only good frequency selectivity, but also offer small size and affordable cost. Passive-circuit solutions have traditionally been relied on to meet pertinent system requirements. For select applications, alternatives are now emerging that make use of recent advances in active-filter techniques. Although microwave active filter concepts have been around for many years, system designers have shown reluctance to employ them, due to a common association with high intrinsic levels of noise and signal distortion. This perception is not always based on sound reasoning.

To objectively assess noise performance of competing passive and active filter approaches, it is important to compare realizations that use similar passive-circuit components, as dissipation losses in the latter tend to be the dominant sources of noise in both cases. An active filter realized, for instance, as a monolithic integrated circuit on a 100-μm-thick GaAs substrate and incorporating planar lumped-circuit elements, should be compared to a passive filter of similar size, also realized with planar lumped elements on a dielectric substrate of the same thickness. Conversely, employing lower loss passive-circuit elements of nonplanar design will provide comparable noise benefits to both passive and active filters alike. As for circuit nonlinear behavior, a passive filter employed in a system front end is typically paired with an amplifier that, in turn, introduces distortion. What ultimately counts are the nonlinear characteristics of the front-end ensemble, assessed for a given overall system design. When evaluated in this context, an active filter, which by itself constitutes an ensemble of passive- and active-circuit functions, can offer competitive performance, in addition to size and cost advantages.

The capabilities of present-day microwave active filters derive from concept-development and feasibility-demonstration efforts that have been pursued over the past three decades. The appended list of references, i.e., [1]–[17], arranged in chronological order, provides a representative sampling of pertinent advances. The goal of this study is to contribute to these advances with a new technique for realizing frequency-tunable channelized notch filters. Their intended use is in frequency-agile applications where rapid adaptation to fast-changing signal conditions is sought. The focus is on minimizing passband noise and eliminating passband distortion through choice of filter architecture.

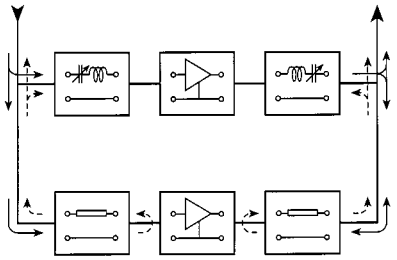

Fig. 1. Block diagram of a two-branch channelized notch filter, with primary and parasitic signal flow directions identified by solid- and dashed-line arrows, respectively.

II. Concept

A channelized active notch filter, in its simplest form, comprises two parallel-connected branches that support signal flow in the forward direction only, with one branch assigned a bandpass response and the other an all-pass response [14]. This is illustrated in the block diagram of Fig. 1, where the bandpass branch comprises an amplifier flanked by two bandpass filter sections. The second branch contains an amplifier and segments of uniform transmission line. Respective blocks are identified by self-explanatory symbols whose purpose is to serve as labels only, without intent to represent complexity and topological detail of pertinent circuit realizations. A rejection notch positioned at the bandpass center frequency is generated through mutual cancellation, at the composite-filter output port, of the signals

Manuscript received October 3, 2000. This work was supported by the Office of Naval Research.

The author is with the Naval Research Laboratory, Washington, DC 20375-5347 USA (e-mail: rauscher@ieee.org).

Publisher Item Identifier S 0018-9480(01)06137-3.

fed forward through the two branches, after arranging for the signals to be of equal amplitude and of opposite phase at the designated notch frequency. Signals at composite-filter passband frequencies are guided through the second branch that serves as the bypass channel and is largely responsible for defining passband characteristics. Frequency tuning of the notch can be achieved, in principle, through incorporation of voltage-variable capacitance elements into the bandpass segments, as alluded to in the figure.

Although the outlined approach works well in fixed-frequency situations, consistent notch rejection becomes difficult to achieve when frequency tuning is actually attempted. This, in part, is due to unavoidable parasitic reflections within the channelized structure, which compromise notch depth by interfering with the cancellation process. The solid-line arrows in Fig. 1 mark the nominal flow directions of signal components under ideal conditions. Among the components is a portion of the signal that exits the bandpass channel, enters the bypass branch in reverse direction by way of the nondirectional output branch junction, and is absorbed in the output stage of the bypass-channel amplifier. In a real-world situation, small reflections off the bypass amplifier's output port, as well as off its input port, will produce parasitic signal flow, represented in Fig. 1 by the dashed-line arrows. The interfering parasitic signals are difficult to neutralize over an appreciable tuning interval, due to inherent differences in phase rotation as a function of frequency among parasitic and desired signal components. Achievable notch depth becomes bounded by amplifier return loss.

Another concern with the configuration of Fig. 1 is the noise and signal distortion generated in the bypass-branch amplifier. As the bypass channel determines the passband characteristics of the notch filter, the presence of the amplifier may be a liability in receiver-front-end applications. Yet, the amplifier cannot be simply omitted, even though it is not generally needed for loss compensation, due to the nonresonant low-loss typical nature of the bypass channel. The amplifier's primary task is to keep signals flowing in the forward direction. The recursive structure that would result from omitting the amplifier would make it difficult to achieve a well-behaved filter response.

The schematic block diagram of Fig. 2 represents a new tunable-notch-filter architecture that overcomes the mentioned concerns [18]. This configuration distinguishes itself through its three feedforward branches, two of which constitute bandpass channels, with the third functioning as the bypass channel. For reasons described below, the bypass branch requires no amplifier. The total number of amplifiers thus remains the same as in the earlier two-branch case. Frequency tunability is achieved through voltage-variable reactance elements incorporated into the bandpass filter segments.

The two bandpass branches, together with the transmission-line sections of the two direct-coupled branches in Fig. 2 that link, respectively, the input and output ports of the bandpass branches, form a nonreciprocal active-circuit rendition of a classic four-port directional bandpass filter. As in the classic case, the two bandpass branches are assigned identical amplitude responses. Pertinent transmission-line lengths are chosen so that the signals transmitted through the two bandpass channels add in-phase at the composite-filter output port, but cancel each other in the opposite-flow direction. The channels' passband centers coincide with the designated notch center frequency of the composite filter. The remainder of the incident signal, whose frequency content falls within the channels' passband, but is not directed to one of the bandpass branches, continues on through the bypass branch, where it is adjusted in phase, and passed on to the output port of the composite filter. There, the signal remainder combines with the amplitude-adjusted in-phase signal components transmitted through the two bandpass channels to effect mutual signal cancellation at the intended notch frequency. The challenge is to maintain, over a given notch tuning interval, correct amplitude and phase relationships among the signals of all three channels so as to render the shape and depth of the resultant transmission notch largely invariant to tuning.

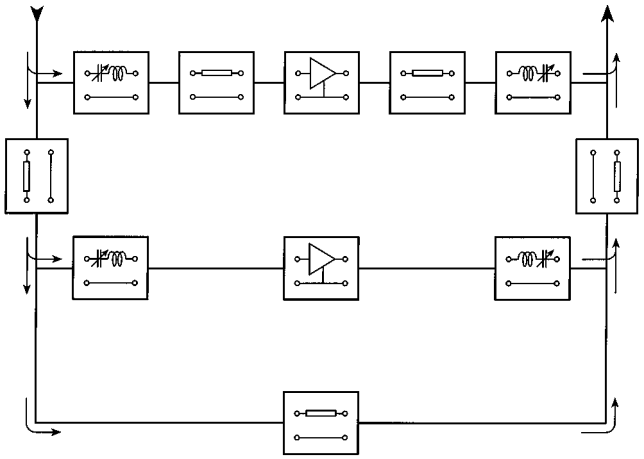

Fig. 2. Block diagram of a new three-branch channelized notch filter with arrows identifying primary signal-flow directions.

Due to the noted attributes of the four-port directional-bandpass-filter assembly, no signals are injected backward into the bypass channel, save for reflections stemming from junction discontinuities and residuals introduced by practical limits on achievable directivity of the four-port assembly. Using standard passive-circuit techniques to reduce parasitic signal components to below-significant levels, an amplifier is no longer needed to ensure forward signal flow in the bypass branch, allowing the latter to be implemented as a passive reciprocal all-pass network. In practice, this network may merely consist of a uniform transmission line. Signals at passband frequencies of the composite notch filter, as a result, can propagate largely unperturbed from the filter's input port to its output port via the bypass-branch transmission line and the direct-coupled branches of the directional bandpass assembly. Thus, noise and signal-distortion levels of the composite filter at frequencies away from the notch become essentially determined by the properties of uniform transmission-line sections. This is illustrated by the experimental example described below.

III. Experimental Circuit

To demonstrate the approach, a channelized three-branch notch filter was designed and implemented as a hybrid-integrated circuit, providing continuous variability of the notch center frequency between 9.5–10.5 GHz. The circuit is depicted

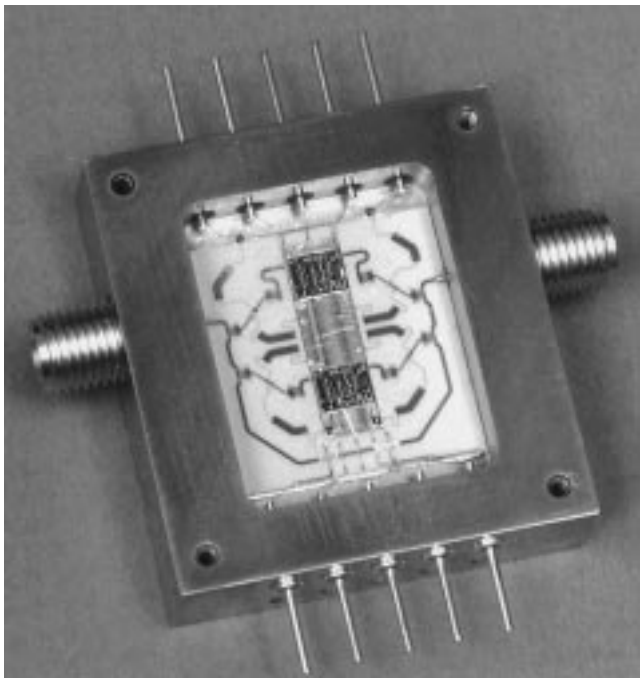

Fig. 3. Varactor-tuned three-channel active notch filter with a 9.5–10.5-GHz tuning range, realized as a hybrid-integrated circuit.

in Fig. 3, with an equivalent-circuit diagram presented in Fig. 4. The latter is only an approximate representation of the circuit's topology, with emphasis on the defining features. The use of same labels for nominally identical network elements serves to underscore the circuit's symmetric properties and basic simplicity, both of which may not be readily apparent from inspection of the circuit topology alone.

The four tunable filter blocks shown in Fig. 2 are realized as capacitively coupled single-resonant bandpass-filter sections. They consist of microstrip structures on 0.010-in-thick alumina substrates, as do all other planar passive-circuit components of the composite filter. With reference to Fig. 4, each of the four electrically identical bandpass sections contains one tuning varactor diode D, series-connected between two equal-length inductive transmission-line segments TL_1, and flanked at both ends by interdigitated coupling capacitors. The latter are augmented by capacitors that are shunt-connected to ground, forming equivalent Π networks represented by capacitors C_1, C_2, and C_3, with respective modeled capacitance values of 0.073, 0.035, and 0.198 pF. The inductive line segments are of nominal 65-Ω characteristic impedance and possess a common electrical length of 49° at 10 GHz. The diode in each bandpass section is a commercial MA-46604 GaAs tuning varactor in discrete-chip form that provides an equivalent series-capacitance tuning range of 0.5–1.6 pF. Connected to each diode terminal is a varactor bias network that is made up of three cascade-connected transmission-line segments that are a quarter-wavelength long at the center of the tuning band, with a 10-pF bypass capacitor to ground at the feed point. The bias networks, employing a high–low–high sequence of characteristic line impedances within the cascade, have negligible influence on filter performance, and were, therefore, not included in the equivalent-circuit representation of Fig. 4. Each bandpass section in itself is electrically symmetric. This empirically chosen feature yields passband widths that are essentially invariant to tuning frequency, a prerequisite for obtaining a composite-filter rejection notch whose shape remains constant across the designated tuning interval.

To complete the directional filter assembly, as indicated in Fig. 4, the four tunable bandpass-filter sections are augmented by two identical amplifiers G, four 50-Ω transmission-line segments TL_2, and eight small series-connected inductors L. The variable-gain amplifiers are monolithic-integrated circuits of type EG-6345 from Texas Instruments Incorporated, Dallas, TX, with a maximum gain of 24.5 dB at 10 GHz. Each of the four transmission-line segments is nominally a quarter-wave long. The inductors are realized as short pieces of 70-Ω transmission line, providing 0.12 nH of equivalent series inductance. They counteract the junction disturbances caused by the predominantly capacitive driving-point impedance characteristics of the directional filter assembly's bandpass sections at off-resonance frequencies, as seen by signals propagating through the direct-coupled arms of the assembly. The inductive compensation and the quarter-wave spacing of the junctions help to reduce calculated residual signal return at the four ports of the directional filter assembly to less than -19 dB, and limit calculated residual signal coupling to the assembly's isolated port to less than -22 dB. These maximum values apply to all passband and stopband frequencies within the 6–14-GHz range of observation, and to all notch-tuning positions. Similar performance could have also been obtained by having the directional bandpass assembly's two direct-coupled branches, instead of its two bandpass channels, differ in electrical length by a half-wavelength.

Augmenting the directional bandpass assembly with transmission-line element TL_3 completes the tunable notch filter. In the physical implementation of Fig. 3, the transmission line spans three different alumina substrates to form the notch filter's bypass channel. The total length of the line is determined by the need to produce, at the designated notch frequency, the sought-after destructive interference among signals passed to the composite-filter output port through the two bandpass channels, and the signal passed to the output port through the bypass channel. The proper amplitude relationship among the three channel signals, for cancellation to occur, is achieved by engaging the gain controls of the bandpass-channel amplifiers to set nominal amplifier gain at 21.5 dB. A special feature of the design is that the amplifier control settings do not have to be adjusted as the filter's constant-width rejection notch is moved across the 9.5–10.5-GHz tuning interval.

IV. Experimental Results

The calculated small-signal performance of the notch filter is shown in Fig. 5 for five different combinations of monotonically adjusted varactor bias voltages. The individual response curves, with a minimum notch depth of 35 dB, exhibit tuning-invariant rejection-notch widths of 70 MHz between the 10-dB-down points. Across the depicted frequency band, the maximum passband insertion loss is 0.8 dB, with a minimum return loss at the notch filter's input and output ports of 18 dB.

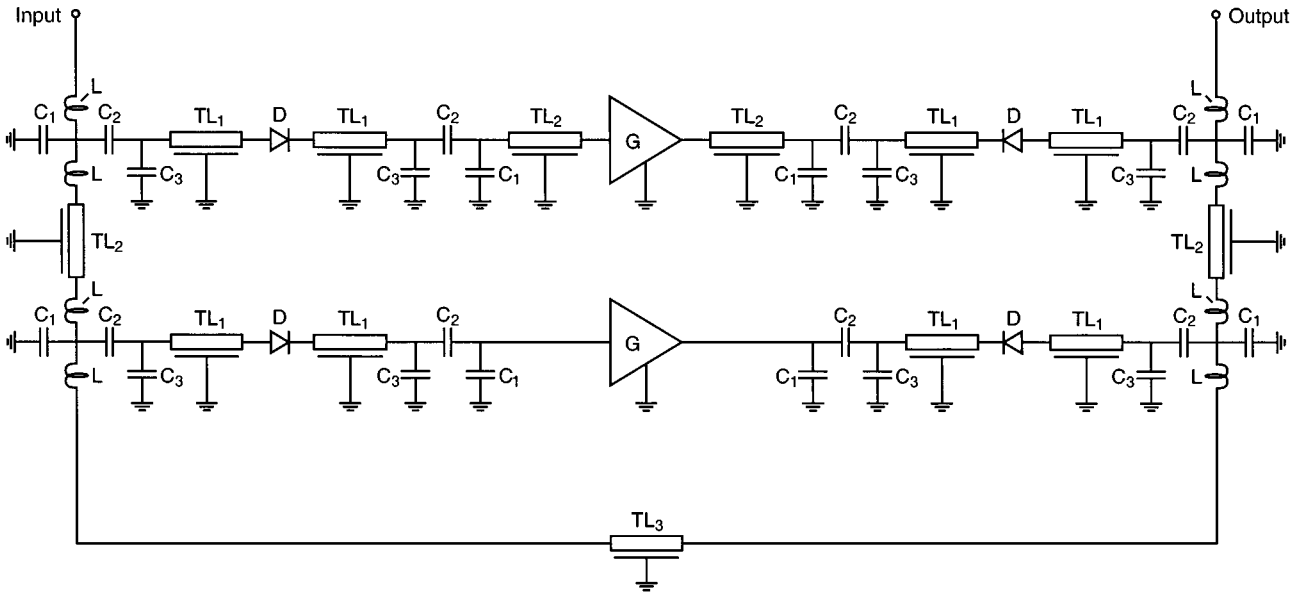

Fig. 4. Simplified equivalent-circuit schematic of the experimental three-channel tunable notch filter.

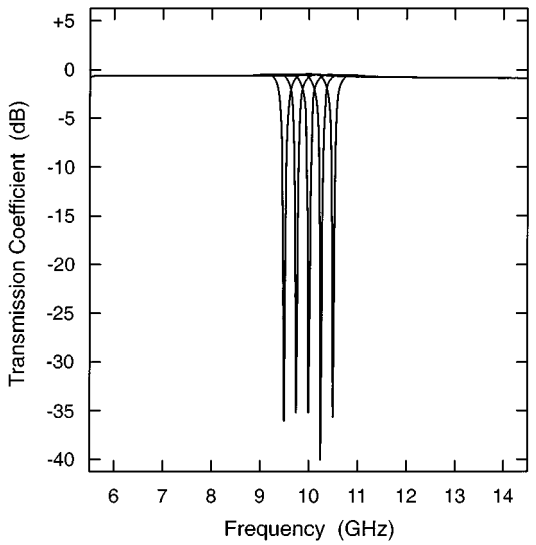

Fig. 5. Calculated small-signal transmission response of the filter for five different notch positions.

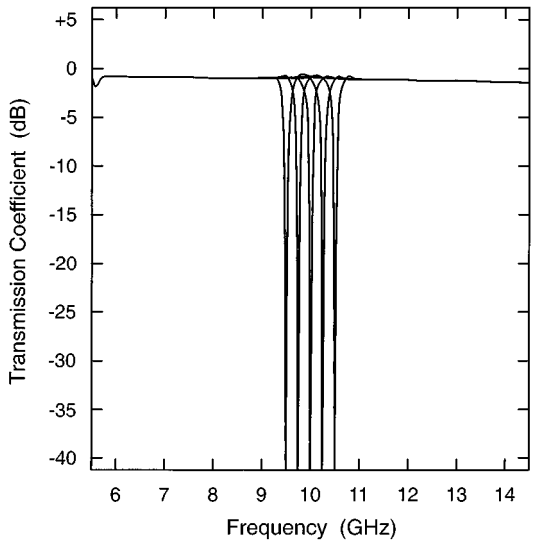

Fig. 6. Measured small-signal transmission response of the filter for five different notch positions.

The measured small-signal characteristics of the filter are plotted in Fig. 6, obtained for varactor bias voltages of 0.5–16 V, and fixed amplifier control settings. The experimental results are in close agreement with the calculated curves, exhibiting the same tuning-independent-bandwidth behavior. Empirical fine adjustment of the varactor voltages permitted recorded rejection notch depths to be increased to over 40 dB across the entire tuning interval. The improvement in performance came as a consequence of having to slightly tweak the varactor voltages for each notch position to correct for small fabrication-related differences between bandpass channel responses. Such differences are attributed to manufacturing variances among discrete semiconductor components, and variances among wire bonds used to connect frequency-sensitive circuit elements within the bandpass-filter sections.

Measured passband insertion loss values, which include contributions from input and output connectors, range from 0.9 dB at 6 GHz to 1.6 dB at 14 GHz. The small dip below 6 GHz and a similar one that occurs around 15 GHz are caused by the varactor bias networks. The dips could have been avoided by resorting to bias networks that involve a single quarter-wavelength segment of high-impedance transmission line instead of the employed three-line combination described earlier. This would have required the use of via holes to connect associated feed-point bypass capacitors to ground, due to topological constraints.

The measured noise performance of the filter, with the rejection notch positioned at 10 GHz, is presented in Fig. 7, depicted by the solid-line curve. As expected, the passband noise figure, within the limitations of the scalar noise-measurement equipment, follows the passband insertion loss curve. In the vicinity

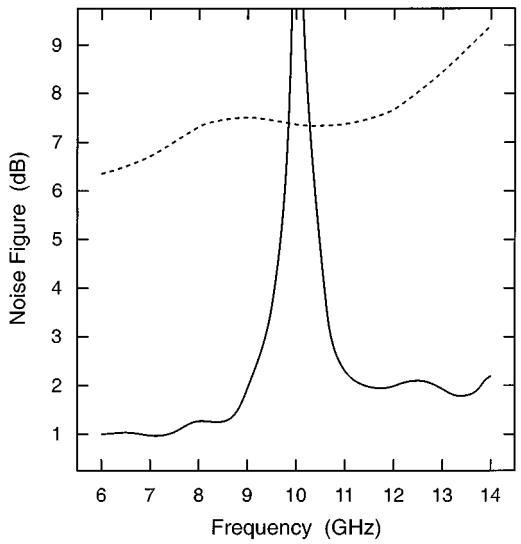

Fig. 7. Measured filter noise performance for the rejection notch positioned at 10 GHz (solid line), together with the measured noise response of a channel amplifier by itself (dashed line).

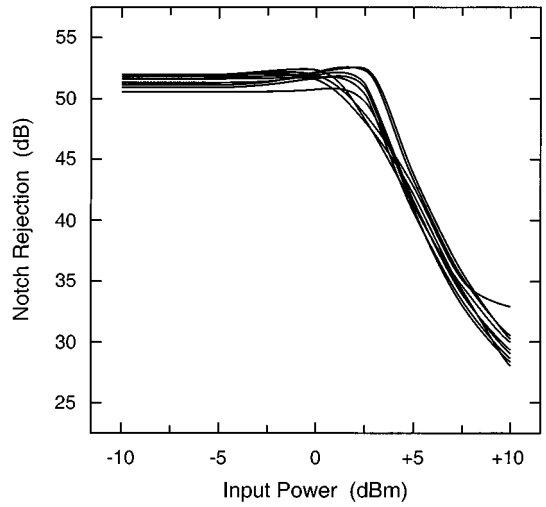

Fig. 8. Measured notch depth as a function of input drive level for seven different notch positions distributed evenly in 125-MHz steps across the 9.5–10.5-GHz tuning interval.

of the notch center, where the signal drops out, the noise figure rises sharply, also as expected. The specific shape of the spike is largely determined by the noise properties of the two-channel amplifiers and by the frequency selectivity of the flanking band-pass-filter sections. The noise contributions of the amplifiers, originally designed for driver applications, are relatively high, as indicated by the measured noise figure of a separate unit from the same manufacturing lot, represented in Fig. 7 by the dashed-line curve. Calculations indicate that the width of the noise spike could be significantly reduced through the use of lower noise amplifiers, should noise in the immediate vicinity of the notch be a concern.

As for filter performance under large-signal conditions, Fig. 8 shows signal rejection at the notch center as a function of incident signal level. Included are seven traces that relate to different notch positions, spaced uniformly across the 9.5–10.5-GHz tuning interval. The curves are tightly clustered,

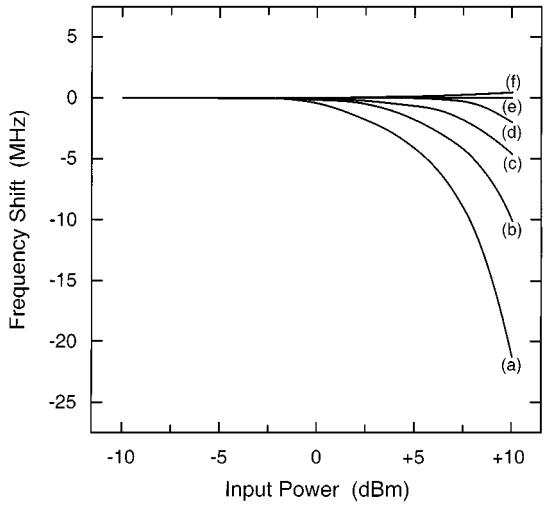

Fig. 9. Measured shift in notch position as a function of input drive level for nominal notch positions at: (a) 9.5 GHz, (b) 9.625 GHz, (c) 9.75 GHz, (d) 9.875 GHz, (e) 10 GHz, and (f) 10.125–10.5 GHz.

whence no attempt was made to label them individually. As could be readily predicted, notch depth decreases with increasing drive level, primarily due to gain saturation in the two amplifiers, but also partially due to the nonlinear properties of the varactors. With the amplifier gain settings kept at their small-signal-optimized values, a minimum notch depth of 40 dB was maintained for input drive levels up to +5 dBm. Out of curiosity, and to confirm that amplifier gain saturation was indeed mainly responsible for compromising notch rejection at elevated drive levels, amplifier gain settings were readjusted at each input drive level, which restored 40-dB notch depths at drive levels up to +7.5 dBm. Except for notch positions in the vicinity of 9.5 GHz, adjusting amplifier gain actually extended the operating range to +10 dBm. Limitations at the low end of the tuning interval were the result of overdriven varactors, biased at the low voltages needed to reach the low end of the interval, thereby engaging nonlinear effects that were larger than could simply be accommodated through increases in amplifier gain.

Varactor-related nonlinear effects are also primarily responsible for causing slight shifts in notch center frequency with increasing input signal level. This is documented in Fig. 9, where such drive-level-dependent shifts are plotted for different nominal tuning positions, with the amplifier gain controls again set for optimized small-signal performance. As is evident from the measured curves, the effects are barely discernible for notch center frequencies in the upper half of the tuning band. The effects are more evident toward the low end of the band, where the capacitance values of the circuit's abrupt-junction varactors are most sensitive to changes in voltage. The voltage dependence gives rise to dynamically averaged capacitance values that are larger than respective small-signal values, progressively lowering frequencies of resonance with an increasing drive level. Still, even in the worst-case situation depicted in Fig. 9, the deviation in the notch position remains less than 5 MHz for an incident signal level up to +5 dBm.

With the notch filter's passband behavior determined by the passive-circuit properties of the transmission-line-based bypass

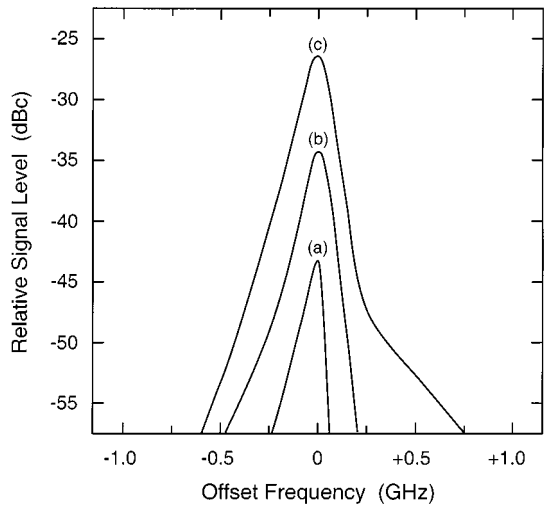

Fig. 10. Measured two-tone intermodulation distortion with the rejection notch positioned at 10 GHz, and for input drive levels of: (a) 0 dBm, (b) +5 dBm, and (c) +10 dBm.

channel, any occurring intermodulation distortion should remain confined to the immediate vicinity of the notch, the only region where amplifiers and tuning varactors fulfill circuit functions and can produce nonlinear signal interaction. This indeed proved to be the case, as confirmed by the results given in Fig. 10, where the third-order intermodulation-distortion products generated by the filter are plotted for three different input signal drive levels. Although the displayed results pertain specifically to the situation where the notch is positioned at 10 GHz, they are representative of distortion behavior encountered across the entire tuning band. The measurements were performed using a two-tone test setup, with one of the tones aligned with the center of the notch, while the other was swept in frequency. The curves depict distortion levels that have been normalized to the common signal level of the two equal-strength incident tones and recorded as a function of frequency separation between the two tones.

V. Conclusion

The frequency-tunable active filter described in this paper was inspired by a need to provide frequency-agile suppression of signal interference in a receiver. An active-circuit approach pursued in conjunction with varactor tuning was chosen in an effort to achieve adequate frequency selectivity and tuning speed, while keeping projected filter size and manufacturing cost to a minimum. The particular channelized architecture was selected to achieve optimum filter transparency at passband frequencies, assure unconditional circuit stability, and exploit the convenience of a modular design methodology. The resultant filter circuit provides a rejection notch that is continuously tunable over a 1-GHz frequency span around 10 GHz, maintaining 40 dB of signal rejection at the notch center for incident signal levels up to +5 dBm. Tuning is accomplished by monotonically varying the bias voltages of four varactor diodes. Special attributes of the filter include very low passband noise and intermodulation distortion, a tuning-invariant rejection-notch width, and the ability to function as described without having to readjust the gain settings of the channel amplifiers at each notch position.

The derivation of the new channelized-notch-filter concept was guided by a desire to minimize filter-generated noise and intermodulation distortion through judicious choice of circuit architecture, confining pertinent concerns to frequencies in the immediate vicinity of the tunable rejection notch. Although the current realization was able to satisfy stipulated objectives, relying solely on available technologies and components, performance improvements beyond what has been demonstrated could be achieved with the help of alternate technologies. Measures to reduce stopband signal distortion and improve sensitivity of notch position to drive level might include, for instance, the replacement of the presently employed abrupt-junction varactor diodes with more linear hyperabrupt-junction variants. In situations where stepwise tunability is acceptable, possible options might also encompass the use of microelectromechanically switched banks of fixed-valued capacitors to achieve even better linearity. Additional distortion- and noise-related stopband benefits could be derived from the insertion of higher dynamic-range gain modules, which might, in the future, involve the exploitation of emergent wide-bandgap-materials technology. At passband frequencies, in contrast, filter performance is largely determined by the characteristics of the filter's bypass channel that contains no semiconductor components, only a few cascade-connected nonresonant sections of a uniform transmission line. Thus, noise at frequencies away from the notch is reduced to levels commensurate with the residual insertion loss of the line segments, and distortion at those frequencies is eliminated altogether, constituting one of the primary distinctions of the described technique.

Acknowledgment

The author would like to thank S. Kirchoefer, Naval Research Laboratory, Washington, DC, and A. Hung, Army Research Laboratory, Adelphi, MD, and D. Martin, Army Research Laboratory, Adelphi, MD, for their assistance with the assembly of the test circuit. The author would also like to acknowledge stimulating discussions with D. Jachowski, Maui Filter Works, Pukalani, HI.

References

[1] D. K. Adams and R. Y. C. Ho, "Active filters for UHF and microwave frequencies," *IEEE Trans. Microwave Theory Tech.*, vol. MTT-17, pp. 662–670, Sept. 1969.

[2] R. V. Snyder and D. L. Bozarth, "Analysis and design of a microwave transistor active filter," *IEEE Trans. Microwave Theory Tech.*, vol. MTT-18, pp. 2–9, Jan. 1970.

[3] W. Jutzi, "Microwave bandwidth active transversal filter concept with MESFETs," *IEEE Trans. Microwave Theory Tech.*, vol. MTT-19, pp. 760–767, Sept. 1971.

[4] C. Rauscher, "Microwave active filters based on transversal and recursive principles," *IEEE Trans. Microwave Theory Tech.*, vol. MTT-33, pp. 1350–1360, Dec. 1985.

[5] M. J. Schindler and Y. Tajima, "A novel MMIC active filter with lumped and transversal elements," *IEEE Trans. Microwave Theory Tech.*, vol. 37, pp. 2148–2153, Dec. 1989.

[6] R. R. Bonetti and A. E. Williams, "An octave-band MMIC active filter," in *IEEE MTT-S Int. Microwave Symp. Dig.*, vol. 2, May 1990, pp. 823–826.
[7] H. Suwaki and T. Ohira, "A very small MMIC variable filter based on a new active filter design concept," in *IEEE GaAs IC Symp. Dig.*, Oct. 1990, pp. 93–96.
[8] X. H. Jiao, P. Guillon, B. Jarry, and B. Madrangeas, "Microwave frequency agile active filters for MIC and MMIC applications," in *IEEE MTT-S Int. Microwave Symp. Dig.*, vol. 1, May 1990, pp. 503–506.
[9] C.-Y. Chang and T. Itoh, "Microwave active filters based on coupled negative resistance method," *IEEE Trans. Microwave Theory Tech.*, vol. 38, pp. 1879–1884, Dec. 1990.
[10] P. Katzin, B. Bedard, and Y. Ayasli, "Narrow-band MMIC filters with automatic tuning and Q-factor control," in *IEEE MTT-S Int. Microwave Symp. Dig.*, vol. 1, June 1993, pp. 403–406.
[11] B. P. Hopf, I. Wolff, and M. Guglielmi, "Coplanar MMIC active bandpass filters using negative resistance circuits," *IEEE Trans. Microwave Theory Tech.*, vol. 42, pp. 2598–2602, Dec. 1994.
[12] S. Lucyszyn and I. D. Robertson, "Monolithic narrow-band filter using ultrahigh-Q tunable active inductors," *IEEE Trans. Microwave Theory Tech.*, vol. 42, pp. 2617–2622, Dec. 1994.
[13] V. Aparin and P. Katzin, "Active GaAs MMIC bandpass filters with automatic frequency tuning and insertion loss control," *IEEE J. Solid-State Circuits*, vol. 30, pp. 1068–1073, Oct. 1995.
[14] C. Rauscher, "Microwave channelized active filters—A new modular approach to achieving compactness and high selectivity," *IEEE Trans. Microwave Theory Tech.*, vol. 44, pp. 122–132, Jan. 1996.
[15] A. Romano and R. R. Mansour, "Enhanced-Q microstrip bandpass filter with coupled negative resistors," in *IEEE MTT-S Int. Microwave Symp. Dig.*, vol. 2, June 1997, pp. 709–712.
[16] H. Ezzedine, L. Billonnet, B. Jarry, and P. Guillon, "Optimization of noise performance for various topologies of planar microwave active filters using noise wave techniques," *IEEE Trans. Microwave Theory Tech.*, vol. 46, pp. 2484–2492, Dec. 1998.
[17] C. Rauscher, "Two-branch microwave channelized active bandpass filters," *IEEE Trans. Microwave Theory Tech.*, vol. 48, pp. 437–444, Mar. 2000.
[18] ——, "A tunable X-band active notch filter with low-distortion passband response," in *IEEE MTT-S Int. Microwave Symp. Dig.*, vol. 1, June 2000, pp. 179–182.

Christen Rauscher (S'73–M'75–SM'82–F'89) received the Diploma degree in electrical engineering and the Doctorate degree from the Swiss Federal Institute of Technology, Zürich, Switzerland, in 1969 and 1975, respectively.

From 1976 to 1978, he studied the nonlinear behavior of GaAs field-effect transistors at Cornell University, Ithaca, NY, and at the Naval Research Laboratory, Washington, DC. He subsequently joined the Naval Research Laboratory, as a Member of the Technical Staff, where he currently heads the Solid-State Circuits Section. On sabbatical leave from 1985 to 1986, he investigated the application of high-speed photoconductor technology to the on-chip characterization of microwave monolithic integrated circuits and millimeter-wave devices at the Los Alamos National Laboratory, Los Alamos, NM. His current research interests are centered on the pursuit of new high-frequency filter concepts and the exploitation of nonlinear signal interaction in semiconductor devices at microwave, millimeter-wave, and optical frequencies.

Dr. Rauscher was the recipient of an international fellowship from the Swiss National Science Foundation, the 1987 IEEE Microwave Prize, the 1991 Naval Research Laboratory Sigma Xi Applied Science Award presented by the Scientific Research Society of America, and the 1999 IEEE Microwave Application Award. He recently completed a three-year term as an IEEE Distinguished Microwave Lecturer.